Review
Korean Circulation J 2005;35:1-14
ISSN 1738-5520
ⓒ 2005, The Korean Society of Circulation

Noninvasive Imaging of Atherosclerotic Plaques Using MRI and CT

Yeon Hyeon Choe, MD

Department of Radiology and Center for Imaging Science, Samsung Medical Center, Sungkyunkwan University School of Medicine, Seoul, Korea

ABSTRACT

Noninvasive, high-resolution MRI has shown its efficacy in the visualization of carotid atherosclerotic plaque characteristics. MRI is the only noninvasive option for thin plaque cap, active inflammation, fissured/injured plaque and intraplaque hemorrhage, is also useful in monitoring the response after statin therapy, and has the potential to image a coronary plaque and to determine its composition. New contrast agents and targeted molecular imaging open a window for MRI detection of thrombi and assessment of atherosclerotic activity and plaque vulnerability. Currently, multidetector CT is capable of the noninvasive detection of coronary stenosis and coronary calcifications. High resolution CT may be beneficial in the detection of noncalcified vulnerable coronary plaques, and more reliable with the use of newer high-speed volume CT scanners. **(Korean Circulation J 2005;35:1-14)**

KEY WORDS : Atherosclerosis ; Tomography, spiral computed ; Magnetic resonance imaging.

Introduction

Conventional angiography has been regarded as the gold standard technique for the detection and diagnosis of arterial stenosis and occlusion. Recently, noninvasive techniques have advanced very rapidly. Fast multidetector-row CT (MDCT) and MRI enable rapid screening of the whole body vascular tree for atherosclerosis. These imaging modalities demonstrate an angiographic display of the vasculature using three-dimensional image reconstruction techniques.[1-4] CT and MRI also provide cross-sectional images of atherosclerotic vessels.[1)2)5)] High-resolution CT and unique tissue contrast of MRI, combined with contrast agent application, may be useful in the characterization of atherosclerotic plaques. It is very important to detect coronary and carotid atherosclerosis before the fatal outcomes of the process appear clinically.

The concept of 'vulnerable plaque' implies that detection of unstable plaques is important in the prevention of future cardiovascular events, because vulnerable plaques may rupture and cause sudden arterial occlusion or distal embolization. Naghavi et al.[6] proposed criteria for defining a vulnerable plaque based on the study of culprit plaques. In their proposal, the major criteria for vulnerable plaque were active inflammation, a thin cap with a large lipid core, endothelial denudation with superficial platelet aggregation, fissured plaque and stenosis >90%, and the minor criteria were a superficial calcified nodule, glistening yellow on angioscopy, intraplaque hemorrhage, endothelial dysfunction and outward remodeling. Therefore, we were urged to find ideal noninvasive methods for atherosclerosis imaging. In this context, MDCT and MRI are most suited for this purpose.

For the detection of most major and minor criteria for plaque vulnerability, MRI and MDCT are noninvasive options. MRI is the only noninvasive option for a thin plaque cap, active inflammation, fissured/injured plaques and an intraplaque hemorrhage.[6] MDCT and MRI are very rapidly evolving, and the future applications of these techniques are promising. The resultant, timely and appropriate intervention of the atherosclerotic process may benefit patients by stabilizing atherosclerotic plaques or restoring the luminal diameter by angioplasty/stenting.

Correspondence : Yeon Hyeon Choe, MD, Department of Radiology and Center for Imaging Science, Samsung Medical Center, Sungkyunkwan University School of Medicine, 50 Ilwon-dong, Gangnam-gu, Seoul 135-710, Korea
Tel : 82-2-3410-2509, Fax : 82-2-3410-2559
E-mail : yhchoe@smc.samsung.co.kr

Noninvasive Modalities for Atherosclerosis Imaging

The carotid artery is a major source of cerebral embolism, and atherosclerosis of the carotid artery reflects the degree of

systemic atherosclerosis. Noninvasive imaging modalities are clinically useful for screening carotid diseases and assessment of the degree of stenosis. Recent developments in ultrasonography (US), MRI and CT have much improved the image quality and diagnostic reliability of each modality. US has been utilized for the noninvasive assessment of carotid stenosis and measurement of the carotid wall thickness. Focal ulceration and change in the echogenicity of the plaque can be visualized with using US. The Doppler technique is useful in the measurement of flow velocity through the stenotic lumen. The Doppler US threshold and criteria for significant carotid stenosis vary according to individual laboratories.[7]

High resolution and contrast of the images are achieved by high frequency transducers (7−13 MHz) and recent developments in imaging techniques, such as tissue harmonic US. The intimomedial thickness is easily measurable by US. However, US has limitations in characterizing the plaque. US has limited anatomical coverage of the internal carotid artery and is more operator-dependent than other techniques.

MRI of Atherosclerosis

Time-of-flight (TOF) MR angiography has been useful in the luminal depiction of intracranial and extracranial carotid arteries. The recently-introduced contrast-enhanced MR angiography is more advantageous in eliminating flow-related artifact and in obtaining 3-dimensional angiographic images with high contrast. High-resolution MRI techniques enable reliable characterization of the plaque, especially in carotid arteries.[8] High-resolution carotid MRI is performed using 3-inch bilateral surface coils (FOV, 10×10 cm; slice thickness, 2−3 mm). Image acquisition includes 3-dimensional TOF MR angiography; T1-weighted pre- and post-contrast spin echo (T1WI) or a double inversion recovery technique, T2-weighted spin echo imaging (T2WI) and T1-weighted fatsaturated spin echo imaging. The components of the plaque can be intracellular lipid and extracellular lipid core, loose connective tissue/collagen matrix/fibrocelluar, calcifications and hemorrhagic components.[9] High-resolution MRI can visualize fibrous cap and focal ulcers, and differentiate fibrocelluar components from the lipid core or hemorrhagic components using a multi-spectral approach (Table 1) (Fig. 1-5).[10-12]

Fibrocellular components and loose connective tissue show modestly high signal intensities (SI) on T2WI (Fig. 1).[8] The lipid core typically shows low SI on T2WI and high SI on T1WI. Hemorrhagic components or thrombi are of variable SI on T2WI (low SI, mostly) and high SI on T1WI with fat saturation (Fig. 2). Infrequently, hydrophilic necrosis shows very high SI on T2WI and low SI on T1WI (Fig. 5). Plaques with friable, gel-like state component may be prone to rupture and embolization. Peculiar findings of this plaque component distinguish it from the fibrocelluar component or lipid-rich area.

MRI classification and characterization of atherosclerotic lesions

According to the study of Cai et al,[13] *in vivo* high-resolution multicontrast MRI was capable of classifying intermediate to advanced atherosclerotic lesions in the human carotid artery and was also capable of distinguishing advanced lesions from early and intermediate atherosclerotic plaques. Using 4 different contrast-weighted images (time of flight and T1-, PD- and T2-weighted), the classification obtained by MRI and the American Heart Association classifications showed good agreement, with a Cohen's kappa value (95% CI) of 0.74 (0.67 to 0.82) and a weighted kappa of 0.79. The sensitivities and specificities of MRI classification were as follows: type I-II lesions, 67 and 100%; type III lesions, 81 and 98%; type IV-V lesions, 84 and 90%; type VI lesions, 82 and 91%; type VII lesions, 80 and 94% and type VIII lesions, 56 and 100%, respectively.

Table 1. MRI appearance of plaque components on various imaging sequences

Plaque components	T2WI	T1WI	Intermediate weighted	TOF	Enhancement on T1WI, postcontrast
Recent hemorrhage	Variable	High to moderate (high with FS)	Variable	High	No
Lipid-rich core	Variable (low, typically)	High (low with FS)	High	Moderate	No
Hydrophilic necrosis	Very high	Low	High	Low	No
Fibrous tissue	Variable (moderate, typically)	Moderate	High	Moderate to low	Yes
Calcification	Low	Low	Low	Low	No

Tissue contrast is relative to SI of muscle. FS: fat-saturation, TOF: time-of-flight MR angiography

Evaluation of fibrous cap

The TOF technique can show the fibrous cap of the plaque as a low signal band along the plaque surface (Fig. 2, 3). Multisequence MRI can accurately characterize the *in vivo* state of the fibrous cap. Hatsukami et al.[10] first described the use of the TOF sequence for fibrous cap imaging *in vivo*. They studied 22 patients with a 3-dimensional multiple overlapping thin slab angiography protocol before carotid endarterectomy. There was a high level of agreement between the MRI and histological findings in 36 sites available for comparison: 89% agreement, kappa (95% CI)=0.83 (0.67 to 1.0) and weighted kappa=0.87 and a Spearman's correlation coefficient of 0.88 (significant to the 0.01 level). Using the TOF MRI technique, they distinguished intact, thick fibrous caps from intact thin and disrupted caps in atherosclerotic carotid arteries *in vivo*. Mitsumori et al.[11] examined presurgical MR images using four contrast weightings (3D time of flight, T1, proton density, and T2) to evidence an unstable fibrous cap in 18 patients. Assessment of the preoperative appearance of the fibrous cap had a high sensitivity (0.81) and specificity (0.90) for identifying an unstable cap *in vivo*. The availability of different contrast weightings facilitated image interpretation when intimal calcifications or flow artifacts obscured the lumen surface.

Trivedi et al.[14] quantified the fibrous cap and lipid core contents proportional to the overall plaque area in 25 symptomatic patients. The intra-class correlation coefficients between two MR readers were 0.94 and 0.88 for quantifying fibrous cap and lipid core components, respectively. There was good agreement between MR and histology derived quantification of both the fibrous cap and lipid core content.

Yuan et al.[15] correlated the state of the fibrous caps with the symptoms of the patients, and showed a strong and significant trend showing a higher percentage of symptomatic patients for ruptured caps (70%) compared with thick caps (9%) (p=0.001). Patients with ruptured fibrous caps were 23 times more likely to have a recent transient ischemic attack or stroke (95% CI=3,210) compared with patients with thick caps.

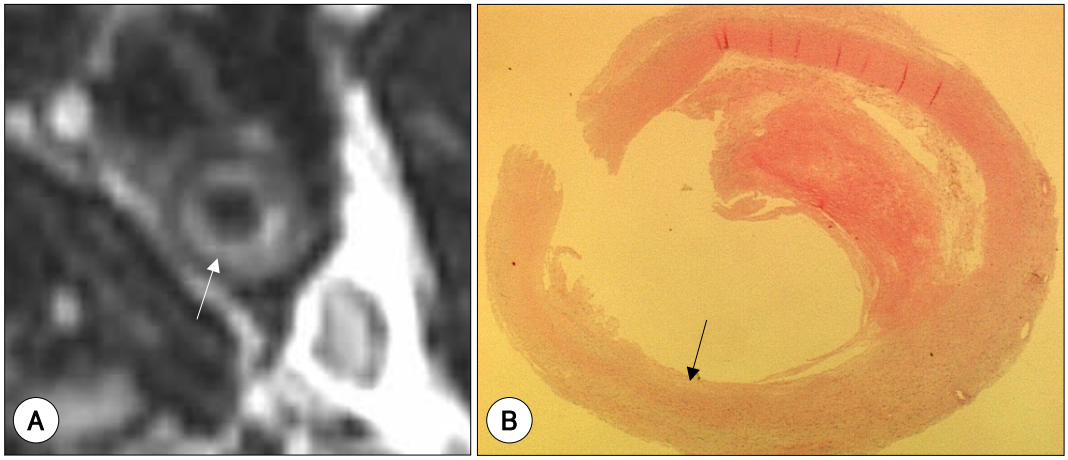

Fig. 1. Fibrous component-dominant plaque in the internal carotid artery. A: high-resolution T2-weighted spin echo MR image, showing a high signal intensity area (arrow) in the inner part of the plaque. B: photomicrograph showing a fibrous component (arrow) in the corresponding area (H & E).

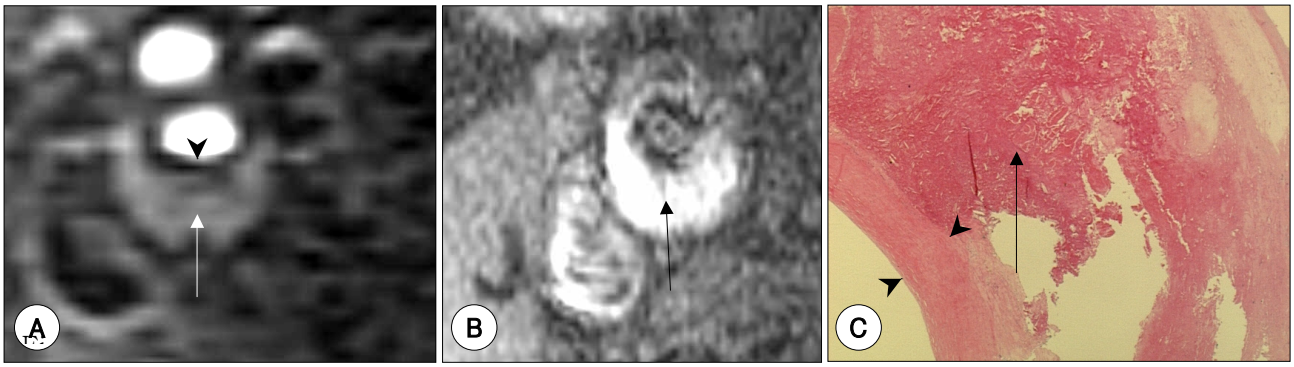

Fig. 2. High-resolution MRI of a hemorrhagic carotid plaque, with an intact fibrous cap. A: source image of TOF MR angiography showing a thick fibrous cap (arrowhead) as a dark signal intensity band. High signal intensity area in the plaque (arrow) suggests intraplaque hemorrhage. B: T1-weighted spin echo image, with fat-saturation, showing high signal intensity (arrow) of the plaque due to hemorrhage. C: photomicrograph showing a thick fibrous cap (arrowheads) and intraplaque hemorrhage (arrow) (H & E).

Intraplaque hemorrhage

High SI in the plaque may suggest a focal area of fresh hemorrhage on TOF images (Fig. 2).[16-18] The presence of an intraplaque hemorrhage may imply increased risk of plaque rupture and distal embolization. According to Chu et al.,[16] MRI detected carotid an intraplaque hemorrhage in 27 patients with high sensitivity (90%), but only moderate specificity (74%). Using the sequences of 3-dimensional TOF, double-inversion recovery, T1WI, PDW and T2WI, two readers grouped hemorrhages into fresh, recent and old categories. A hemorrhage was histologically identified and staged in 145/189 (77%) of carotid artery plaque locations.

In vivo high-resolution MRI can detect and differentiate an intraplaque hemorrhage from a juxtaluminal hemorrhage/thrombus with good accuracy. According to Kampschulte et al.,[17] the sensitivity and specificity for MRI to correctly identify cross sections containing a hemorrhage were 96 and 82%, respectively, in 26 patients. MRI was able to distinguish a juxtaluminal hemorrhage/thrombus from an intraplaque hemorrhage, with an accuracy of 96%. The distribution of lesion types underlying hemorrhages differed significantly (p=0.004). Intraplaque hemorrhages had an underlying lipid-rich type IV/V lesion in 55% of histological sections, whereas juxtaluminal hemorrhages/thrombi had an underlying calcified lesion type VII in 70% of sections. The association of a hemorrhage and lesion types suggests potential differences in origin.

Cappendijk et al.[18] also investigated the performance of high-resolution T1-weighted (T1w) turbo field echo (TFE) magnetic resonance imaging (MRI) for the identification of intraplaque hemorrhages in 11 patients. More than 80% of the histologically proven intraplaque hemorrhages could be

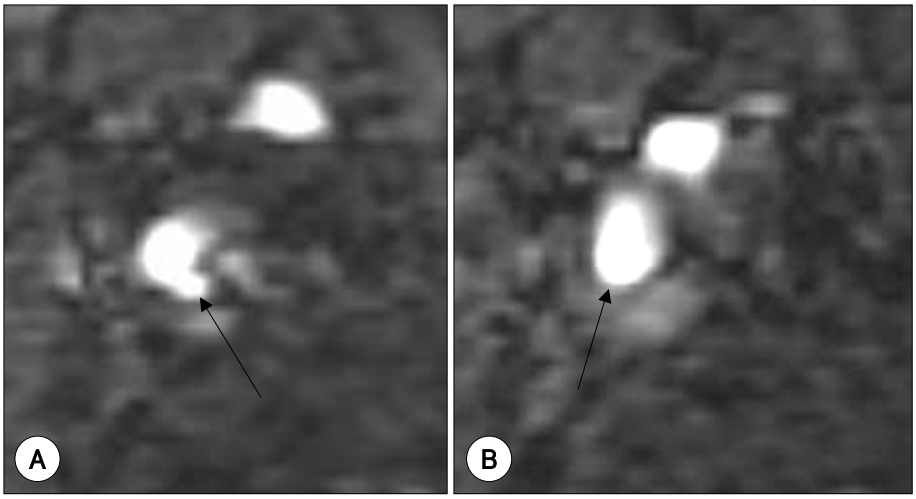

Fig. 3. Examples of an ulcerated plaque (A) and a thin fibrous cap (B) of the internal carotid artery on source images from TOF MR angiography. A: arrow indicates defect in the fibrous cap. B: arrow indicates thinning of the fibrous cap.

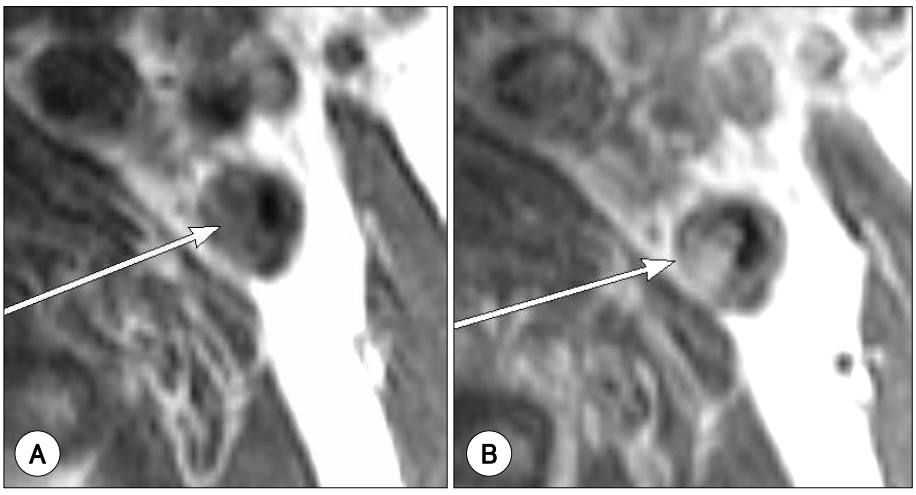

Fig. 4. Contrast enhancement of the plaque (arrows) suggests increased vascularity in the fibrous component of the plaque. A: pre-contrast T1-weighted spin echo image. B: post-contrast (intravenous injection of Gd-DTPA, 10 mL) T1-weighted spin echo image.

detected using the TFE sequence, with high interobserver agreement (Kappa=0.73).

Gd-DTPA-enhanced imaging

Gd-DTPA-enhanced MRI may differentiate necrotic or lipid-rich components from fibrous components, as the former do not show enhancement, but the latter do (Fig. 4).[19] Enhancement after injection of a conventional contrast agent, Gd-DTPA, indicates increased vascularity in the plaque. Paradoxically, increased vascularity may mean an increased degree of inflammation and ongoing active atherosclerosis. Plaques with increased vascularity are subject to increased risk of an intraplaque hemorrhage. According to Yuan et al.,[19] there were statistically significant differences in the mean intensity change between tissues before and after contrast injection, with the largest increase for the fibrous tissue (79.5%) and the smallest for a necrotic core (28.6%). Additionally, histological analysis showed that a subset of fibrous regions, rich in plaque neovascularization, could be identified using a threshold of 80% enhancement (sensitivity, 76%; specificity, 79%).

Kerwin et al.[20] measured the neovasculature volume in carotid atherosclerotic plaques using a kinetic model. Dynamic contrast-enhanced MRI provided an indication of the extent of the neovasculature within carotid atherosclerotic plaques. They estimated the fractional blood volume and compared it with fractional microvascular area on histological staining with ULEX and CD-31. The correlation coefficient for the two measurement was 0.80 ($p<0.001$).

The MRI characteristics of the aorta and carotid arteries may be associated with elevated serum markers of inflammation, frequently in the absence of a definite atheroma. Weiss et al.[21] compared the MRI findings with serum markers for systemic inflammation. Double inversion recovery, fast spin-echo images of the common carotid arteries and infrarenal aorta were obtained at 1.5 T, both before and after gadolinium-DTPA, in 52 subjects ≥40 years of age. Twenty-two study participants had increases in wall thicknesses (n=14), T2-weighted signal intensities (n=11) and/or contrast enhancement values (n=7) >2 standard deviations of the control group mean values. Ten subjects in this group had evidence of focal plaques in the carotids (n=5) and/or aorta (n=6). Compared with the remaining 30 subjects, these 22 had significantly higher levels of interleukin-6, C-reactive protein, vascular cell adhesion molecule-1 and intercellular adhesion molecule-1, but no significant differences in the levels of E-selectin.

Accuracy of MRI plaque imaging

Multispectral MRI can identify the lipid-rich necrotic core in human carotid atherosclerosis *in vivo*, with high sensitivity and specificity. Yuan et al.[12] compared 90 *in vivo* MRI cross sections with matched histological sections of the endarterectomy specimen in 18 patients. Using 4 contrast weightings (T1, T2, proton density, and 3D TOF), the MR images of the vessel wall were examined for the presence of a lipid-rich necrotic core and/or intraplaque hemorrhage. The overall accuracy (95% CI) of multispectral MRI was 87% (80 to 94%), with sensitivity and specificity of 85 (78 to 92%) and 92% (86 to 98%), respectively. There was good agreement between the MRI and histological findings, with a value of kappa=0.69 (0.53 to 0.85).

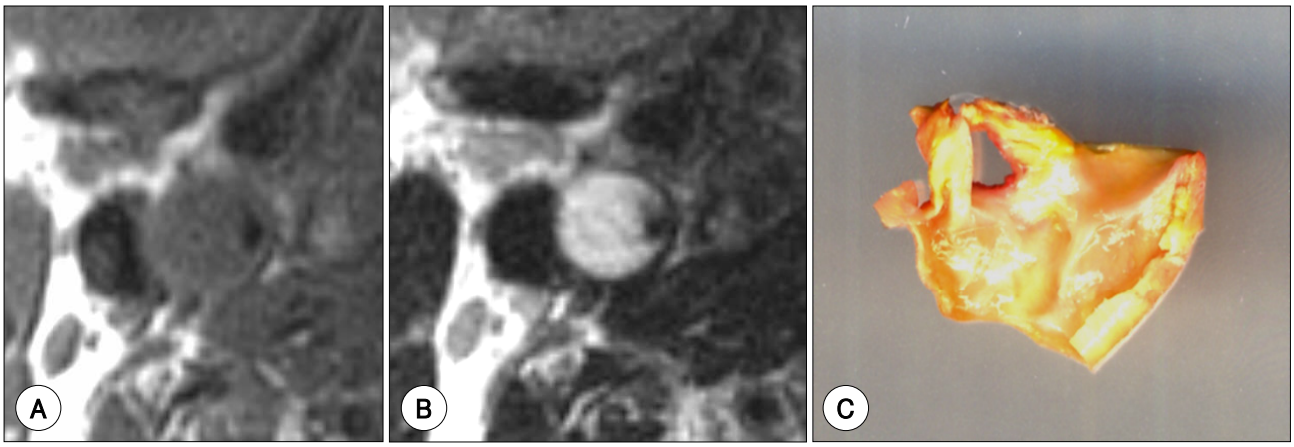

Fig. 5. Gel-like, hydrophilic necrosis of the carotid plaque. A: T1-weighted spin echo image showing a low signal intensity of the plaque. B: T2-weighted spin echo image showing a bright signal intensity of the plaque, suggestive of the high water content of this plaque. C: carotid endarterectomy specimen showing the gel-like state of the plaque content.

MRI monitoring of the response after statin therapy

High-resolution carotid MRI can provide useful information on the therapeutic response to lipid-lowering drugs.[22-27] Measurements of the plaque thickness, area, volume, stenosis degrees and characters of plaque components can be compared before and after medical treatment. The treatment plan can be decided from the initial plaque MRI findings. Vulnerability of the plaques, rather than the degree of stenosis, may count more toward the surgical/interventional treatment of carotid stenosis.

McConnell et al.[22] observed regression of atherosclerosis 12 to 20 months after withdrawal of a cholesterol diet and the progression of the atherosclerosis in rabbits with a continued high cholesterol diet by T2WI. The plaque thickness decreased significantly in the low-cholesterol group (0.60±0.05 mm at 20 months versus 0.85±0.06 mm at 4 months, p=0.006), with a trend toward an increase in the high-cholesterol group (1.02±0.08 mm at 20 months versus 0.85±0.06 mm at 4 months, p=0.1). Helft et al.[23] observed regression or progression of lipid components in the plaque on serial MRI. MRI of the aorta was performed 3 times: baseline, after atherosclerosis induction (9 months old), and after atherosclerosis regression or progression (15 months old). There was a significant (p<0.001) reduction in the lipidic component of plaques in the regression group, an increase in the progression group, and a significant decrease in the fibrotic composition of lesions in the progression group. A significant correlation (p<0.001) was found between the MRI and histopathology for the atherosclerotic burden and plaque composition.

Corti et al.[24] observed regression of carotid and aortic atherosclerotic lesions (44 aortic and 32 carotid artery plaques) in 21 asymptomatic hypercholesterolemic patients after maintained lipid-lowering therapy with Simvastatin for 24 months. The effects of statin on these atherosclerotic lesions were evaluated as changes versus the baseline lumen area (LA), vessel wall thickness (VWT) and vessel wall area (VWA) by MRI. Maximal reductions in the plasma total and LDL cholesterols by Simvastatin (23% and 38% respectively; p<0.01 versus baseline) were achieved after approximately 6 weeks of therapy, and maintained thereafter throughout the study. Significant (p<0.01) reductions in the maximal VWT and VWA at 12 months (10 and 11% for aortic and 8 and 11% for carotid plaques, respectively), without changes in the LA, have been reported. Further decreases in the VWT and VWA, ranging from 12 to 20%, were observed at 18 and 24 months. A slight, but significant, increase (ranging from 4 to 6%) in the LA was seen in both carotid and aortic lesions at these later time points.

According to Corti et al.,[25] the anti-atherogenic effects of a selective peroxisomal proliferator-activated receptor-gamma (PPAR-gamma) agonist and Simvastatin, as well as their combination, were demonstrated in cholesterol-fed rabbits by MRI after treatment for 6 months. In rabbits treated with Simvastatin or Simvastatin plus a PPAR-gamma agonist showed significant plaque regression (−12±4% [p<0.05] and −22±4% [p<0.01], respectively) by MRI plaque area measurements. The regression was independent of the plasma lipid levels. Histopathological analysis showed decreased macrophage content and matrix metalloproteinase activity, but an increased smooth muscle cell/collagen content of lesions.

Lima et al.[26] measured atherosclerotic plaques in the thoracic aorta by combined surface/transesophageal MRI in 27 patients, both before and after 6 months of Simvastatin therapy (20 to 80 mg daily). The plaque volume and luminal dimensions were measured in 6 cross sections used to construct a 2.4-cm 3D volume of the aorta, including the plaque and lumen. The plaque volume was reduced from 3.3±1.4 to 2.9±1.4 cm^3 at 6 months (p<0.02). The plaque regression (plaque volume/area reduction) was significantly related to the LDL cholesterol reduction (p<0.02 and p<0.005, respectively).

In our institution, 45 patients with 30−70% sonographic carotid stenosis were treated daily with 20 mg of Simvastatin. They were followed up for 19±7.5 months. In 7 patients (16%), increased fibrous content or plaque cap thickness on multispectral MRI suggested plaque stabilization. There was significant change in the plaque thickness after medical treatment (4.2 mm±1.0 vs. 3.4 mm±1.3, p<0.001) (unpublished data) (Fig. 6).

Coronary artery wall imaging

Contrast arteriography can not directly image plaques. Noninvasive, high-resolution magnetic resonance has the potential to image coronary plaques.[28-34] Fayad et al.[28] used a black-blood MRI (BB-MR) method, free of motion and blood-flow artifacts, for high-resolution (down to 0.46 mm in-plane resolution and 3-mm slice thickness) imaging of the coronary artery lumen and wall. The difference in the maximum wall thickness between the 8 normal subjects [0.75±0.17 mm (range, 0.55 to 1.0 mm)] and 5 patients with

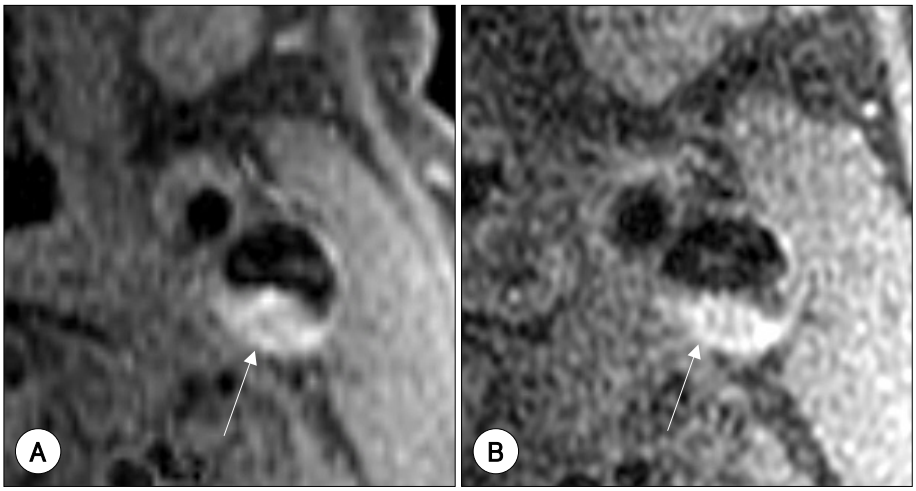

Fig. 6. The effect of lipid-lowering therapy, as demonstrated by MRI. Pre- (A) and post-treatment high-resolution MRI (B) after 12 months Simvastatin (20 mg daily) medication, showing a 0.5 mm decrease in the thickness of the carotid plaque.

≥40% stenosis [localized wall thickness of 4.38±0.71 mm (range, 3.30 to 5.73 mm)] was statistically significant ($p<0.0001$).

Free-breathing 3D black-blood coronary MRI, with isotropic resolution, identified an increased coronary vessel wall thickness, with preservation of the lumen size, in patients with nonsignificant coronary artery disease. This approach showed potential to quantify subclinical diseases. Botnar et al.[30] used a 3D approach, together with a novel local inversion technique, to facilitate more extensive coverage. The combination of a nonselective inversion prepulse with a 2D selective local inversion prepulse allowed for the suppression of an unwanted signal outside a user-defined region of interest. Among 10 subjects evaluated using 3D-spiral readout, the local inversion pulse effectively suppressed the signal from ventricular blood, myocardium and chest wall tissue in all cases. The coronary vessel wall could be visualized within the entire imaging volume.

Kim et al.[31] evaluated high-resolution black-blood 3D MRI on a 1.5 T scanner for *in vivo* visualization of the proximal coronary artery vessel wall in 6 clinically healthy subjects and 6 patients with nonsignificant coronary artery disease. Free-breathing 3D coronary vessel wall imaging was performed along the major axis of the right coronary artery, with isotropic spatial resolution ($1.0\times1.0\times1.0$ mm^3), using black-blood spiral image acquisition. MRI visualized the contiguous proximal right coronary artery in all subjects. Both the mean vessel wall thickness (1.7 ± 0.3 versus 1.0 ± 0.2 mm) and wall area (25.4 ± 6.9 versus 11.5 ± 5.2 mm^2) were significantly increased in the patients compared with the healthy subjects (both $p<0.01$).

Differentiation of fibrocellular, lipid-rich and calcific regions is feasible using MRI, as shown in a study on ex vivo coronary arteries.[32] The findings of each component of coronary arteries were similar to those found for the carotid arteries in the previous literature.

Botnar et al.[33] demonstrated the feasibility of intravascular free-breathing black blood coronary vessel wall imaging using a double inversion fast spin echo technique after x-ray guided placement of an internal receiver coil in, or in close proximity to, the target vessel, with reproducible image quality. With internal coil placement in the left circumflex coronary artery, images of the left anterior descending vessel wall appeared similar or superior to those of commercially available phased array surface coil images.

Recently, clinical 3 T scanners have become available. With higher field strengths, coronary vessel wall imaging is likely to benefit from the remarkable gain in signal-to-noise ratio. Botnar et al.[34] demonstrated the feasibility of *in vivo* human high field (3 T) coronary vessel wall imaging, using a free-breathing black blood fast gradient echo technique, with respiratory navigator gating and real-time motion correction.

Contrast agents and molecular MRI approach

Ultrasmall superparamagnetic particles of iron oxide (USPIO; Sinerem, Laboratoire Guerbet, Paris, France) can migrate through the interendothelial junctions and capillary pores, because of the small size of the agent and its long half-life in the blood. Ruehm et al.[35] demonstrated iron uptake in the macrophages embedded in atherosclerotic plaque of hyperlipidemic rabbits using MR angiography 5 days after a USPIO injection. The USPIO contrast agent caused marked

susceptibility effects (spotty signal voids) in the aortic wall. USPIO in the actively phagocytosing cells signifies the presence of active inflammation in the plaque. Therefore, the agent is expected to be useful in the detection of atherosclerosis before luminal stenosis becomes evident.

Kooi et al.[36] observed significant signal decrease in the regions of interest on T2*-weighted MR images 24 hours after administration of Sinerem (2.6 mg Fe/kg) in patients with carotid atheromas. On histopathological and electron microscopic examinations, the USPIO was located primarily in the macrophages within the plaques in 10 of 11 patients, and was found in 75% (27/36) of ruptured or rupture-prone lesions and 7% (1/14) of stable lesions. Signal changes on post-USPIO MRI T2*-weighted gradient echo images were seen in 54% (67/123) of quadrants after 24 hours and 35% (19/55) of quadrants after 72 hours. Schmitz et al.[37] also observed USPIO uptake in human atherosclerotic walls. They found areas of profound signal loss in abdominal aorta and iliac arteries in 7 of 19 elderly patients 24 hour after an intravenous injection of Sinerem (2.6 mg Fe/kg). The optimal time window for imaging of USPIO-induced SI reductions was between 24 and 36 hours, decreasing after 48 hours, but SI reduction was still evident up to 96 hours after infusion.[37] According to Trivedi et al.,[38] areas of signal intensity reduction, corresponding to USPIO/macrophage-positive histological sections, were visualized in 7 of 8 patients given Sinerem (2.6 mg/kg).

Litovsky et al.[39] demonstrated cytokine-induced recruitment of monocyte into aortic atherosclerotic plaques using superparamagnetic iron oxide particles (SPIO, Feridex, Berlex Laboratories) (1 mmol/kg iron injected over 3 min). Feridex was injected into female apo E knockout mice after intraperitoneal injections of cytokines (tissue necrosis factor-α, interleukin-1β, interferon-γ). Histological studies were performed 6 days later. The atherosclerotic plaques in cytokine-treated mice contained more iron-positive macrophages per cross-section than sham-treated apo E knockout mice (42 ± 11.8 vs. 11.6 ± 5.9, $p<0.0001$). The authors believed that iron-laded macrophages in the cytokine-treated mice were newly recruited monocytes, and that initiation of new atherosclerotic plaques may be apparent microscopically. Therefore, USPIO- or SPIO-enhanced MRI may be considered to have potential for detecting active atherosclerosis.

Another experimental contrast material, Gadofluorine M (Schering AG, Berlin, Germany), is a lipophilic, macrocyclic gadolinium-based contrast agent with a perfluorinated side chain. Gadofluorine creates its own interface by forming very small aggregates or micelles in dilute solution. The fluorinated side chain is hydrophobic. Gadofluorine showed specific delayed enhancement in the atheroma of Watanabe heritable hyperlipidemic rabbits (WHHL). According to Barkhausen et al.,[40] delayed enhancement occurred in the aortic wall of WHHL examined with Gadofluorine, but not in the vessel wall of animals with Magnevist (Gd-DTPA; Schering AG, Berlin, Germany) or the control group. The gadolinium concentration was 368 ± 30 nmol/g in aortic walls with plaques in WHHL and 7 ± 5 nmol/g in normal aortic walls. Sirol et al.[41] developed a new pulse sequence for early imaging, instead of a 48 hour delay. A combination of inversion-recovery and diffusion flow-nulling preparatory pulse gradient echo sequence (IR-DIFF-TFL) suppressed the aortic luminal signal, with higher signal intensity 1 hour after injection than with conventional IR-TFL. They also found Gadofluorine to have high affinity for lipid-rich areas.

The mechanism of accumulation of Gadofluorine in the atheroma is unclear, but explanations include; slow leakage of contrast agent into the plaque, with altered endothelial permeability, accumulation in the enlarged interstitial space, necrotic areas and lipid plaque components, and phagocytosis by macrophages or other active transport.[40][41] Binding of the contrast material with denatured protein is also speculated. The advantage of Gadofluorine enhancement is that of positive contrast with visualization on T1WI and a high signal-to-noise ratio (Fig. 7). The clinical benefit of this agent is its ability to detect atherosclerotic plaques very early.

Recently, fibrin-targeted paramagnetic lipid-encapsulated perflouro-carbon nanoparticles were introduced.[42] This agent targets fibrin in the thrombi overlying the vulnerable plaque, not the plaque itself. Fibrin clots targeted *in vitro* with paramagnetic nanoparticles showed highly detectable T1-weighted enhancement. Botnar et al.[43] demonstrated that Gd-DTPA-labeled fibrinogen clots appeared as bright hot spots on the black-blood inversion-recovery TFE sequence. A coronary in-stent thrombus was also visible as high signal intensity on the black-blood inversion-recovery TFE sequence after an intracoronary injection of 60 μmol EP-2104R (EPIX Medical, Inc) over 3 min in swine. In their earlier experiment, Botnar et al.,[44] found that fibrin-targeted agent is useful in noninvasive *in vivo* MRI of acute and subacute thrombosis following a plaque rupture in an animal model of atherosclerosis. In the early stage of coronary thrombosis, thrombi are rich in platelets and fibrin. Therefore, detection of acute

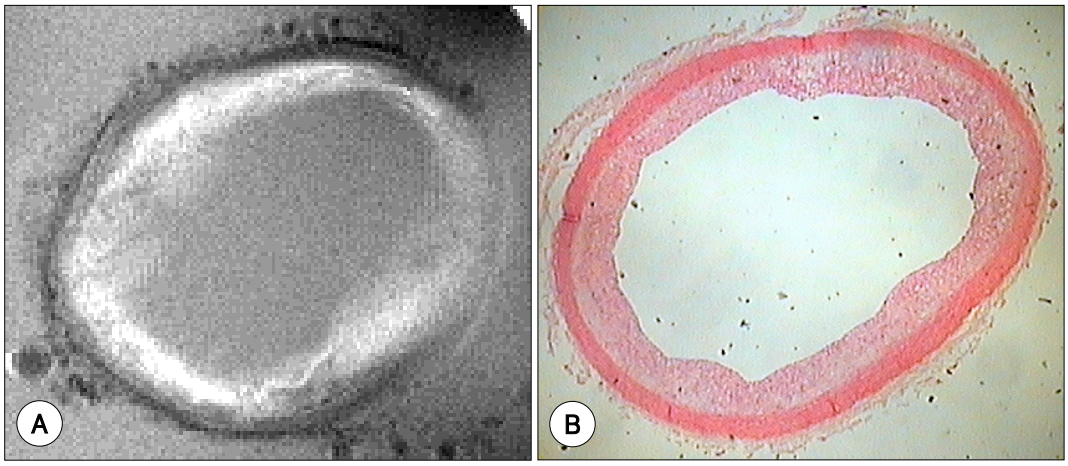

Fig. 7. Aorta of the cholesterol-fed diabetic rabbit, 2 days after Gadofluorine M injection. A: fat-saturated T1-weighted image, obtained with an 8 mm field-of-view on 14-T micro MR equipment (Bruker, Germany), shows high SI areas in the plaque suggestive of Gadofuorine uptake. B: photomicrography of the specimen, showing a circumferential atheroma of a rabbit aorta (×12.5, H & E). Courtesy of Whal Lee, MD, Seoul National University Hospital.

coronary thrombosis is feasible with the fibrin-targeted agent. According to Johansson et al.,[45] the ability to visualize clots was highly dependent on the spatial resolution of the images. An in-plane resolution of at least 0.2×0.2 mm^2 was required for *in vivo* clot visualization after contrast enhancement.

Myeloperoxidase (MPO), which is secreted by activated neutrophils and macrophages, is a potential MRI target for atheroma imaging, as MPO secretion correlates well with a plaque rupture. Chen et al.[46] demonstrated MPO activity in enzyme solutions and in a model tissue system, using a lead compound consisting of a covalent conjugate of GdDOTA and serotonin.

Integrin $\alpha_v\beta_3$ is a marker for angiogenesis and; therefore, represents an attractive target for molecular imaging aimed at the early identification of vulnerable plaques. Winter et al.[47] developed a nanoparticle targeted against integrin $\alpha_v\beta_3$ by incorporating peptide-like particles into its lipid outer layer, which was linked to gadolinium-DTPA. By intravenous injection of a nanoparticle-Gd-DTPA targeted against integrin $\alpha_v\beta_3$ in atherosclerotic cholesterol-fed rabbits they detected increased angiogenesis as a $47 \pm 5\%$ enhancement in the MRI signal averaged throughout the wall of an abdominal aorta. Pretreatment of atherosclerotic rabbits with $\alpha_v\beta_3$-targeted nonparamagnetic nanoparticles competitively blocked specific contrast enhancement of the $\alpha_v\beta_3$-targeted paramagnetic nanoparticles. Histology and immunohistochemistry confirmed marked proliferation of angiogenic vessels within the aortic adventitia, coincident with prominent, neointimal proliferation among cholesterol-fed, atherosclerotic rabbits compared with the sparse incidence of neovasculature in the control animals. The detection of integrin $\alpha_v\beta_3$ by MRI may serve as a useful signature of early atherosclerosis, although the role of integrin $\alpha_v\beta_3$ is unclear in the expansion of the vasa vasorum. With the clinical adoption of 3 T MRI, higher resolution of images should improve neovascular localization.

Ligand-targeted nanoparticles may be useful in site-specific drug delivery for early atherosclerotic lesions, as well as in monitoring the changes in the lesions after medical treatment. Lanza et al.[48] used tissue factor-targeted nanoparticles, containing doxorubicin or paclitaxel, targeted to vascular smooth muscle cells (VSMC), which significantly inhibited their proliferation in cultures over the subsequent 3 days. Targeting of the nanoparticles to VSMC surface epitopes significantly increased the nanoparticle antiproliferative effectiveness, particularly that of paclitaxel. *In vitro* dissolution studies revealed that nanoparticle drug release persisted for over a week. The targeted antiproliferative results were dependent on the hydrophobic nature of the drug and the noncovalent interactions with other surfactant components. Molecular imaging of the nanoparticles adherent to the VSMC was demonstrated with high-resolution T1-weighted MRI at 4.7T. They concluded that targeted paramagnetic nanoparticles might provide a quantifiable drug delivery system for the prevention of restenosis after angioplasty.

Multidetecor CT

The recently developed high speed CT technique (multidetector-row CT) provides improved z-direction spatial and

time resolutions. Stenotic lesions and adjacent anatomic landmarks (e.g., cervical bones) are visualized simultaneously on reconstructed images. MDCT has the capability of noninvasive detection and characterization of coronary artery plaques and thrombi (Fig. 8-10) (Table 2). The lipid core of the plaque is easily characterized, with a dark density in the plaque (Fig. 8).

CT detection and measurement of coronary artery calcium

Without injection of a contrast agent, CT clearly visualizes calcifications and coronary calcifications can be quantified.[49] Their presence and extent correlates to the presence and amount of coronary atherosclerotic plaques. Prospective studies have demonstrated a high predictive value concerning the occurrence of coronary artery disease events and overall mortality.[50] Calcium scoring by CT may be clinically useful in patients at intermediate risk for coronary artery disease events.

Shaw et al.[51] followed up a cohort of 10,377 asymptomatic individuals undergoing cardiac risk factor evaluation and coronary calcium screening with electron-beam CT. The risk-adjusted relative risk values for coronary calcium were 1.64, 1.74, 2.54 and 4.03 for scores of 11−100, 101−400, 401−1,000 and greater than 1,000, respectively ($p<0.001$ for all values), compared with that for a score of 10 or less. Five-year risk-adjusted survivals were 99.0 and 95.0% for calcium scores of 10 or less and of greater than 1,000 ($p<0.001$), respectively. This study shows that coronary calcium provides

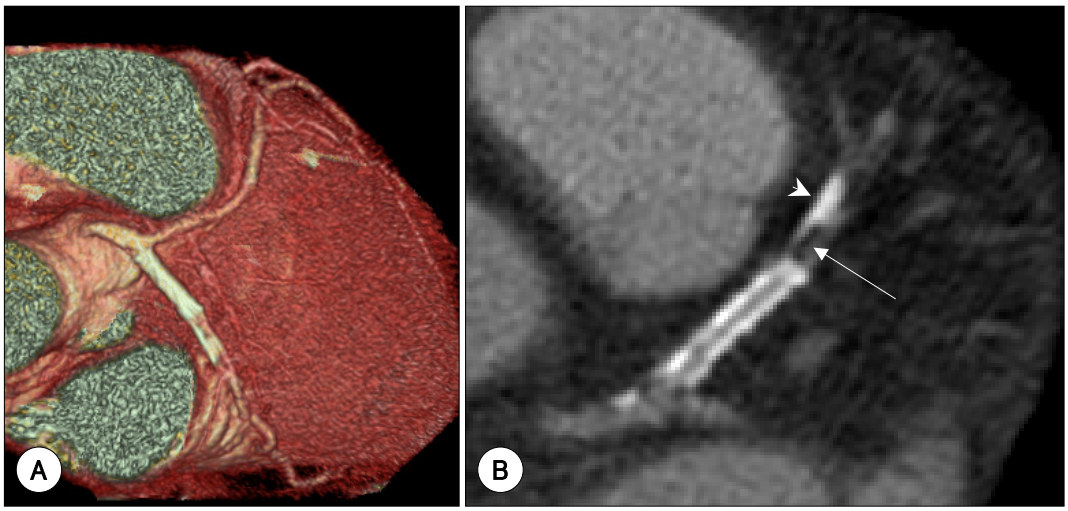

Fig. 8. MDCT demonstrates a fatty plaque (arrow), seen as an area of very low attenuation, along with calcification (arrowhead) distal to a stent in the left anterior descending branch. A: volume-rendered image of the heart. B: axial MDCT image (0.625 mm slice thickness).

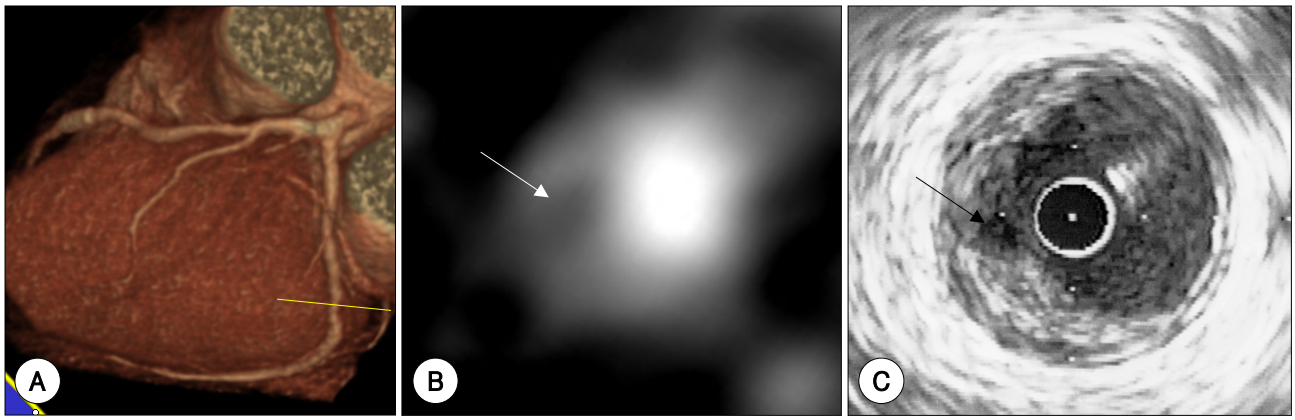

Fig. 9. MDCT and intravascular ultrasound (IVUS) demonstration of coronary artery noncalcified plaque. A: volume-rendered MDCT image, showing mild focal narrowing in the distal segment of the left circumflex artery (crossed by a line). B: reformatted CT image, corresponding to the line on the volume-rendered image, showing an eccentric noncalcified plaque in the coronary arterial wall. The measured CT number of the central low density area (arrow) of the plaque was about 20 HU, suggestive of the presence of a lipid-rich core. C: IVUS image obtained in the same area showing an anechoic area in the wall, confirming the lipid-rich component of the plaque. Courtesy of Joon Beom Seo, MD, Asan Medical Center.

Table 2. CT measurement of atherosclerotic plaque components

Authors	Materials	Number of materials	Lipid-rich or hypoechoic regions[a] (HU)	Fibrous-dominant or hyperechoic region[b] (HU)	Calcific region (HU)	p between *a* and *b*
Nikolaou et al.[32]	Human coronary artery, *ex vivo*	28 lesions in 13 hearts	47±13	82±29		<0.01
Becker et al.[55]	Human coronary artery, *ex vivo*	40 lesions in 11 hearts	47±9	104±28		<0.01
Viles-gonzalez et al.[52]	Rabbit	6	51±25	116±27		<0.01
Schroeder et al.[56]	Human coronary artery, against IVUS	34 plaques in 15 patients	14±26	91±21	419±194	<0.0001
Leber et al.[58]	Human coronary artery, against IVUS	58 vessels in 37 patients	49±22	91±22	391±156	<0.02

HU: hounsfield onit, IVUS: intravascular ultrasound

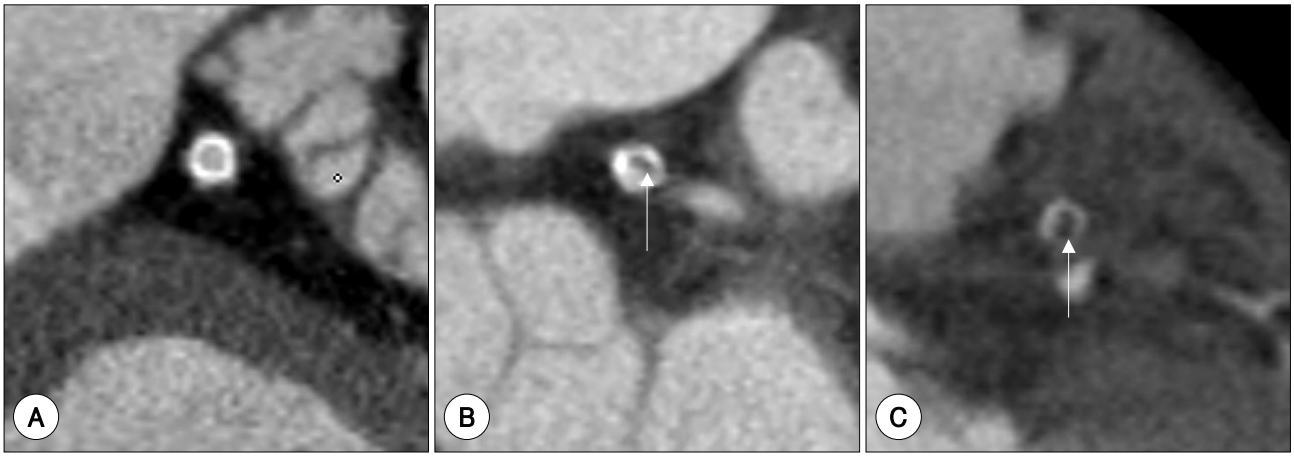

Fig. 10. Short-axial reconstructed images of MDCT show stent restenosis and a thrombus. A: patent stent lumen. B: partial obstruction of the stent with restenosis (arrow). C: stent occlusion with thrombosis (arrow).

independent incremental information in the prediction of all causes of mortality.

MDCT versus MRI in the detection and measurement of atherosclerosis

MDCT correlated well with MRI for the detection and measurement of atherosclerotic lesions. According to an experimental study,[52] in 6 cholesterol-fed rabbits, there was excellent agreement between 3-mm axial reconstructions of 16-slice MDCT and MRI for measurements of vessel wall areas and diameters. The sensitivities and specificities of MDCT and MRI were 89 and 77% and 97 and 94%, respectively, in the detection of atherosclerosis. The interobserver agreements, as determined by κ, were 0.81 and 0.87 for MDCT and MRI, respectively. There was a significant difference in the CT densities between the two components ($p<0.01$) (Table 2). However, it was difficult to distinguish the lipid-rich from the fibrous areas within the same atherosclerotic lesion on the CT images.

Nikolaou et al.[53] compared MDCT and MRI in human *ex vivo* coronary arteries. MDCT was performed with an isotrophic voxel size of 0.6 mm^3, and the MRI with an in-plane resolution of 195 μm, with a 3 mm thickness. Of 28 atherosclerotic lesions, 21 and 23 lesions were found by MDCT and MRI, respectively. There were 4 and 3 false positive cases on MDCT and MRI, respectively, with sensitivities of 75 and 82% for MDCT and MRI. Although the differentiation of AHA type III, IV and Va plaques was difficult using MDCT, there was a significant difference between the mean CT density of predominantly lipid-rich (n=10, HU=47±13) and predominantly fibrous plaques (n=11, HU=87±29) ($p<0.01$). Using MRI, lipid-rich or fibrocellular regions could be well distinguished. Thus, both MDCT and MRI were able to differentiate the typical morphologic features of fatty, fibrous or calcified plaque components.

MDCT detection and characterization of plaque components

Contrast-enhanced MDCT permits the accurate identification of coronary plaques, with the CT density values measured within plaques reflecting the plaque composition. *In vivo* and *ex vivo* MDCT show significantly different attenuation values among the plaque components (Table 2).[54-58]

Schroeder et al.[54] compared the *ex vivo* 16-slice CT and histological findings in 9 human popliteal artery specimens. Although calcified and non-calcified lesions could be differentiated, the diagnostic accuracy by further subclassifying non-calcified plaques as lipid rich and fibrotic was low. In another *ex vivo* study,[55] the mean attenuation was 47±9 HU for lipid-rich plaques and 104±28 HU for fibrous plaques. Leber et al.[58] compared MDCT with intracoronary ultrasound for the detection and characterization of coronary atherosclerotic plaques in 68 vessels of 37 patients. The MDCT-derived density measurements within coronary lesions revealed significantly different values for hypoechoic, hyperechoic and calcified plaques (Table 2). MDCT correctly classified 62 of 80 (78%) sections containing hypoechoic plaque areas, 87 of 112 (78%) sections containing hyperechoic plaque areas and 150 of 158 (95%) sections containing calcified plaque tissue. In 484 of 525 (92%) sections, atherosclerotic lesions were correctly excluded.

Achenbach et al.[59] compared MDCT with intravascular ultrasound in 22 patients. For the detection of segments with any plaque, MDCT had sensitivity and specificity of 82 (41 of 50) and 88% (29 of 33), respectively. For calcified plaques, the sensitivity and specificity were 94 (33 of 36) and 94% (45 of 47), respectively. Coronary segments containing noncalcified plaques were detected with a sensitivity and specificity of 78 (35 of 45) and 87% (33 of 38), respectively, but the presence of exclusively noncalcified plaques was detected with a 53% sensitivity (8 of 15) only.

According to an *ex vivo* study,[60] micro CT is feasible for analysis of the human coronary artery wall. The remarkably high spatial resolution (pixel size, 2 μm) with very thin sections (6 μm section thickness) of 80-kV micro CT (Sky-Scan, 1072; Sky-Scan, Aartselaar, Belgium) enabled calculations of the vessel wall perimeter, and plaque, calcified, lumen and media areas. Micro CT provided quantitative information about the plaque morphology, equivalent to that provided by histomorphometric analysis. Micro CT was able to visualize and characterize areas with different histological predominance. Using gray-scale differences, lesions could be classified as plaque areas with and without smooth muscle cells, and lipid-rich and calcified areas. Thus, micro CT should be considered as an additional tool for *ex vivo* analysis of atherosclerosis.

Data on the accuracy of MDCT plaque detection, quantification of plaque volume and discrimination of lipid-rich from fibrous plaques are still limited. The prognostic significance of noncalcified coronary atherosclerotic plaque detection is unclear. Furthermore, there is significantly high radiation exposure with coronary artery imaging using the current MDCT technique. The effective dose using a 16-slice CT is 8.8 mSv (120 kVp, 370 mA, 0.42 sec exposure time),[61] while that of diagnostic coronary angiography ranges from 3 to 6 mSv.[62] However, high-resolution CT is advantageous for the noninvasive detection and characterization of early coronary atherosclerosis. Future development of flat-panel detector CT will lead to more reliable detection of noncalcified, vulnerable plaques in proximal coronary arteries and significant stenosis in distal segments.

Summary

High-resolution MRI can noninvasively help to identify a vulnerable carotid plaque. Changes in the plaque burden or characters of its components can be quantitatively monitored using this technique. The detection and characterization of coronary artery plaques and calculation of the coronary artery plaque volume may be feasible using high-field (3 T) MRI equipment. With the aid of molecular imaging techniques, including newer contrast agents, MRI will be able to visualize vulnerable atherosclerotic lesions more specifically and sensitively in the future. The current MDCT technique reliably shows calcified coronary lesions, and has the potential to detect noncalcified, vulnerable lesions.

REFERENCES

1) Schoenhagen P, Halliburton SS, Stillman AE, et al. *Noninvasive imaging of coronary arteries: current and future role of multidetector row CT. Radiology 2004;232:7-17.*
2) Schoepf UJ, Becker CR, Ohnesorge BM, Yucel EK. *CT of coronary artery disease. Radiology 2004;232:18-37.*
3) Kim WY, Danias PG, Stuber M, et al. *Coronary magnetic resonance angiography for the detection of coronary stenoses. N Engl J Med 2001;345:1863-9.*
4) Flamm SD, Muthupillai R. *Coronary artery magnetic resonance angiography. J Magn Reson Imaging 2004;19:686-709.*
5) Choudhury RP, Fuster V, Badimon JJ, Fisher EA, Fayad ZA. *MRI and characterization of atherosclerotic plaque. Emerging applications and molecular imaging. Arterioscler Thromb Vasc Biol 2002; 22:1065-74.*
6) Naghavi M, Libby P, Falk E, et al. *From vulnerable plaque to vulnerable patient: a call for new definitions and risk assessment strategies: Part I. Circulation. 2003;108:1664-72.*
7) Choe YH. *Ultrasonographic diagnosis of the carotid abnormalities. J Korean Soc Med Ultrasound 2000;19:151-9.*
8) Yuan C, Mitsumori LM, Beach KW, Maravilla KR. *Carotid atherosclerotic plaque: noninvasive MR characterization and identification of vulnerable lesions. Radiology 2001;221:285-99.*
9) Serfaty J-M, Chaabane L, Tabib A, Chevallier J-M, Briguet A,

Douek PC. *Atherosclerotic plaques: classification and characterization with T2-weighted high-resolution MRI-an in vitro study. Radiology 2001;219:403-10.*
10) Hatsukami TS, Ross R, Polissar NL, Yuan C. *Visualization of fibrous cap thickness and rupture in human atherosclerotic carotid plaque in vivo with high-resolution magnetic resonance imaging. Circulation 2000;102:959-64.*
11) Mitsumori LM, Hatsukami TS, Ferguson MS, Kerwin WS, Cai J, Yuan C. *In vivo accuracy of multisequence MR imaging for identifying unstable fibrous caps in advanced human carotid plaques. J Magn Reson Imaging 2003;17:410-20.*
12) Yuan C, Mitsumori LM, Ferguson MS, et al. *In vivo accuracy of multispectral magnetic resonance imaging for identifying lipidrich necrotic cores and intraplaque hemorrhage in advanced human carotid plaques. Circulation 2001;104:2051-6.*
13) Cai JM, Hatsukami TS, Ferguson MS, Small R, Polissar NL, Yuan C. *Classification of human carotid atherosclerotic lesions with in vivo multicontrast magnetic resonance imaging. Circulation 2002 10;106:1368-73.*
14) Trivedi RA, U-King-Im J, Graves MJ, et al. *Multi-sequence in vivo MRI can quantify fibrous cap and lipid core components in human carotid atherosclerotic plaques. Eur J Vasc Endovasc Surg 2004;28:207-13.*
15) Yuan C, Zhang SX, Polissar NL, et al. *Identification of fibrous cap rupture with magnetic resonance imaging is highly associated with recent transient ischemic attack or stroke. Circulation 2002;105:181-5.*
16) Chu B, Kampschulte A, Ferguson MS, et al. *Hemorrhage in the atherosclerotic carotid plaque: a high-resolution MRI study. Stroke 2004;35:1079-84.*
17) Kampschulte A, Ferguson MS, Kerwin WS, et al. *Differentiation of intraplaque versus juxtaluminal hemorrhage/thrombus in advanced human carotid atherosclerotic lesions by in vivo magnetic resonance imaging. Circulation 2004;110:3239-44.*
18) Cappendijk VC, Cleutjens KB, Heeneman S, et al. *In vivo detection of hemorrhage in human atherosclerotic plaques with magnetic resonance imaging. J Magn Reson Imaging 2004; 20:105-10.*
19) Yuan C, Kerwin WS, Ferguson MS, et al. *Contrast-enhanced high resolution MRI for atherosclerotic carotid artery tissue characterization. J Magn Reson Imaging 2002;15:62-7.*
20) Kerwin W, Hooker A, Spilker M, et al. *Quantitative magnetic resonance imaging analysis of neova-sculature volume in carotid atherosclerotic plaque. Circulation 2003;107:851-6.*
21) Weiss CR, Arai AE, Bui MN, et al. *Arterial wall MRI characteristics are associated with elevated serum markers of inflammation in humans. J Magn Reson Imaging 2001;14:698-704.*
22) McConnell MV, Aikawa M, Maier SE, Ganz P, Libby P, Lee RT. *MRI of rabbit atherosclerosis in response to dietary cholesterol lowering. Arterioscler Thromb Vasc Biol 1999;19: 1956-9.*
23) Helft G, Worthley SG, Fuster V, et al. *Progression and regression of atherosclerotic lesions. Monitoring with serial noninvasive magnetic resonance imaging. Circulation 2002;105: 993-8.*
24) Corti R, Fuster V, Fayad ZA, et al. *Lipid lowering by Simvastatin induces regression of human atherosclerotic lesions: two years' follow-up by high-resolution noninvasive magnetic resonance imaging. Circulation 2002;106:2884-7.*
25) Corti R, Osende JI, Fallon JT, et al. *The selective peroxisomal proliferator-activated receptor-gamma agonist has an additive effect on plaque regression in combination with Simvastatin in experimental atherosclerosis: in vivo study by high-resolution magnetic resonance imaging. J Am Coll Cardiol 2004;43:464-73.*
26) Lima JA, Desai MY, Steen H, Warren WP, Gautam S, Lai S. *Statininduced cholesterol lowering and plaque regression after 6 months of magnetic resonance imaging-monitored therapy. Circulation 2004;110:2336-41.*
27) Zhao XQ, Yuan C, Hatsukami TS, et al. *Effects of prolonged intensive lipid-lowering therapy on the characteristics of carotid atherosclerotic plaques in vivo by MRI: a case-control study. Arterioscler Thromb Vasc Biol 2001;21:1623-9.*
28) Fayad ZA, Fuster V, Fallon JT, et al. *Noninvasive in vivo human coronary artery lumen and wall imaging using black-blood magnetic resonance imaging. Circula-tion 2000;102: 506-10.*
29) Botnar RM, Stuber M, Kissinger KV,. *Noninvasive coronary vessel wall and plaque imaging with magnetic resonance imaging. Circulation 2000;102:2582-7.*
30) Botnar RM, Kim WY, Bornert P, Stuber M, Spuentrup E, Manning WJ. *3D coronary vessel wall imaging utilizing a local inversion technique with spiral image acquisition. Magn Reson Med 2001;46:848-54.*
31) Kim WY, Stuber M, Bornert P, Kissinger KV, Manning WJ, Botnar RM. *Three-dimensional black-blood cardiac magnetic resonance coronary vessel wall imaging detects positive arterial remodeling in patients with nonsignificant coronary artery disease. Circulation 2002;106:296-9.*
32) Nikolaou K, Becker CR, Muders M, et al. *Multidetector-row computed tomography and magnetic resonance imaging of atherosclerotic lesions in human ex vivo coronary arteries. Atherosclerosis 2004;174:243-52.*
33) Botnar RM, Bucker A, Kim WY, Viohl I, Gunther RW, Spuentrup E. *Initial experiences with in vivo intravascular coronary vessel wall imaging. J Magn Reson Imaging 2003;17:615-9.*
34) Botnar RM, Stuber M, Lamerichs R, et al. *Initial experiences with in vivo right coronary artery human MR vessel wall imaging at 3 tesla. J Cardiovasc Magn Reson 2003;5:589-94.*
35) Ruehm SG, Corot C, Vogt P, Kolb S, Debatin JF. *Magnetic resonance imaging of atherosclerotic plaque with ultrasmall superparamagnetic particles of iron oxide in hyperlipidemic rabbit. Circulation 2001;103:415-22.*
36) Kooi ME, Cappendijk VC, Cleutjens KBJM, et al. *Accumulation of ultrasmall superparamagnetic particles of iron oxide in human atherosclerotic plaques can be detected by in vivo magnetic resonance imaging. Circulation 2003;107:2453-8.*
37) Schmitz SA, Taupitz M, Wagner S, Wolf K-J, Beyersdorff D, Hamm B. *Magnetic resonance imaging of atherosclerotic plaques using superparamagnetic iron oxide particles. J Magn Reson Imaging 2001;14:355-61.*
38) Trivedi RA, U-King-Im JM, Graves MJ, et al. *In vivo detection of macrophages in human carotid atheroma: temporal dependence of ultrasmall superparamagnetic particles of iron oxide-enhanced MRI. Stroke 2004;35:1631-5.*
39) Litovsky S, Madjid M, Zarrabi A, Casscells SW, Willerson JT, Naghavi M. *Superparamagnetic iron oxide-based method for quantifying recruitment of monocytes to mouse atherosclerotic lesions in vivo: enhancement by tissue necrosis factor-alpha, interleukin-1beta, and interferon-gamma. Circulation 2003;107: 1545-9.*
40) Barkhausen J, Ebert W, Heyer C, Debatin J, Weinmann H. *Detection of atherosclerotic plaque with Gadofluorine-enhanced magnetic resonance imaging. Circulation 2003;108: 605-9.*
41) Sirol M, Itskovich VV, Mani V, et al. *Lipid-rich atherosclerotic plaques detected by Gadofluorine-enhanced in vivo magnetic resonance imaging. Circulation 2004;109:2890-6.*
42) Flacke S, Fischer S, Scott MJ, et al. *Novel MRI contrast agent*

for molecular imaging of fibrin: implications for detecting vulnerable plaques. Circulation 2001;104:1280-5.

43) Botnar RM, Buecker A, Wiethoff AJ, et al. *In vivo magnetic resonance imaging of coro-nary thrombosis using a fibrinbinding molecular magnetic reso-nance contrast agent. Circulation 2004;110:1463-6.*

44) Botnar RM, Perez AS, Witte S, et al. *In vivo molecular imaging of acute and subacute thrombosis using a fibrin-binding magnetic resonance imaging contrast agent. Circulation 2004;109:2023-9.*

45) Johansson LO, Bjϕrnerud A, AhlstrÖm, Ladd DL, Fujii DK. *A targeted contrast agent for magnetic resonance imaging of thrombus: implications of spatial resolution. J Magn Reson Imaging 2001;13:615-8.*

46) Chen JW, Pham W, Weisledder R, Bogdanov A. *Human myeloperoxidase: a potential target for molecular MRI in atherosclerosis. Magn Reson Med 2004;52:1021-8.*

47) Winter PM, Morawski AM, Caruthers SD, et al. *Molecular imaging of angiogenesis in earlystage atherosclerosis with alpha (v)beta3-integrin-targeted nanoparticles. Circulation. 2003;108:2270-4.*

48) Lanza GM, Yu X, Winter PM, et al. *Targeted antiproliferative drug delivery to vascular smooth muscle cells with a magnetic resonance imaging nanoparticle contrast agent: implications for rational therapy of restenosis. Circulation 2002;106:2842-7.*

49) Agatston AS, Janowitz WR, Hildner FJ, Zusmer NR, Viamonte M, Detrano R. *Quantification of coronary artery calcium using ultrafast computed tomography. J Am Coll Cardiol 1990;15:827-32.*

50) Wexler L, Brundage B, Crouse J, et al. *Coronary artery calcification: pathophysiology, epidemiology, imaging methods, and clinical implications. A statement for health professionals from the American Heart Association. Circulation 1996;94:1175-92.*

51) Shaw LJ, Raggi P, Schisterman E, Berman DS, Callister TQ. *Prognostic value of cardiac risk factors and coronary artery calcium screening for all-cause mortality. Radiology 2003;228:826-33.*

52) Viles-Gonzalez JF, Poon M, Sanz J, et al. *In vivo 16-slice, multidetector-row computed tomography for the assessment of experimental atherosclerosis: comparison with magnetic resonance imaging and histopathology. Circulation 2004;110:1467-72.*

53) Nikolaou K, Becker CR, Muders M, et al. *Multidetector-row computed tomography and magnetic resonance imaging of atherosclerotic lesions in human ex vivo coronary arteries. Atherosclerosis 2004;174:243-52.*

54) Schroeder S, Kuettner A, Wojak T, et al. *Non-invasive evaluation of atherosclerosis with contrast enhanced 16 slice spiral computed tomography: results of ex vivo investigations. Heart 2004;90:1471-5.*

55) Becker CR, Nikolaou K, Muders M, et al. *Ex vivo coronary atherosclerotic plaque characterization with multi-detector-row CT. Eur Radiol 2003;13:2094-8.*

56) Schroeder S, Kopp AF, Baumbach A, et al. *Noninvasive detection and evaluation of atherosclerotic coronary plaques with multislice computed tomography. J Am Coll Cardiol 2001;37:1430-5.*

57) Kopp AF, Schroeder S, Baumbach A, et al. *Non-invasive characterisation of coronary lesion morphology and composition by multislice CT: first results in comparison with intracoronary ultrasound. Eur Radiol 2001;11:1607-11.*

58) Leber AW, Knez A, Becker A, et al. *Accuracy of multidetector spiral computed tomography in identifying and differentiating the composition of coronary atherosclerotic plaques: a comparative study with intracoronary ultrasound. J Am Coll Cardiol 2004;43:1241-7.*

59) Achenbach S, Moselewski F, Ropers D, et al. *Detection of calcified and noncalcified coronary atherosclerostic plaque by contrastenhanced, submillimeter multidetector spiral computed tomography. A segment-based compa-rison with intravascular ultrasound. Circulation 2004;109:14-7.*

60) Langheinrich AC, Bohle RM, Greschus S, et al. *Atherosclerotic lesions at micro CT: feasibility for analysis of coronary artery wall in autopsy specimens. Radiology 2004;231:675-81.*

61) Flohr TG, Schoepf UI, Kuettner. *Advances in cardiac imaging with 16-section systems. Acad Radiol 2003;10:386-401.*

62) Bae KT, Hong C, Whiting BR. *Radiation dose in multidetector row computed tomography cardiac imaging. J Magn Reson Imaging 2004;19:859-63.*